The Clay Minerals Society Workshop Lectures Series, Vol. 21 (2016), Chapter 2, 15–31

COMBINED USE OF NEUTRON-SCATTERING, FLUID-INVASION, AND IMAGE-ANALYSIS TECHNIQUES TO ASSESS PORE STRUCTURE, ACCESSIBILITY, AND CONNECTIVITY IN TIGHT ROCK

CHRISTOPHER R. CLARKSON* and NISAEL A. SOLANO

Department of Geoscience, University of Calgary, 2500 University Drive NW, Calgary, Alberta, Canada T2N 1N4
**e-mail: clarksoc@ucalgary.ca*

Low-permeability (unconventional) reservoirs exhibit heterogeneities at multiple scales that affect flow. While macro-scale heterogeneities are typically evaluated using well-test or production-analysis techniques, core-scale (and finer) analyses are relied upon to evaluate micro-and nano-scale heterogeneities. Pore structure is a known control on flow at the core scale; for unconventional reservoirs, however, pore-size distributions, pore accessibility, and connectivity are challenging to evaluate.

In the present study, a combination of neutron-scattering methods, fluid invasion, and imaging techniques were used to evaluate the degree of pore accessibility and connectivity in a tight oil reservoir within the Cardium Fm. of western Canada. In previous work, cm- to sub-cm scale variations in lithology (elementary lithological components, or ELCs) have been shown to affect flow at the core scale significantly and that reservoir quality varies with the ELCs. The fundamental controls on flow within these ELCs (*i.e.* at the pore scale), however, are poorly understood. The aim of the present study was to gain insight into these controls.

Small-angle and ultra-small angle neutron scattering (SANS/USANS) has revealed that while the Cardium samples exhibit a wide range in pore-size distribution, the accessibility of pores varies significantly with pore size. In particular, the large pore fraction seems to be less accessible than the small pore fraction, which is counter-intuitive. Mercury intrusion data partially support this finding. High-resolution scanning electron microscopy (SEM) imaging suggests that pores within mineral grains may indeed be disconnected/isolated. The SANS/USANS interpretations are based on a simple 2-component (pores + average mineral phase) model, however; detailed mineral mapping reveals that several components may affect significantly the scattering behavior which leads to the conclusion that a multi-phase model may be more appropriate, and that use of the conventional 2-phase model could lead to errors in calculated pore-size distributions and the percentage of disconnected porosity.

1. Introduction

The storage and flow of fluids from low-permeability (tight) unconventional reservoirs, such as shales, is affected by structures and heterogeneities occurring at the field- to nano-scale. Efforts to characterize reservoir properties affecting fluid storage and flow in these reservoirs must, therefore, utilize a wide range of technologies, with different

DOI: 10.1346/CMS-WLS-21.2

resolutions, from field to laboratory scale (Figure 1). These characterization efforts are necessary to assist with the placement and performance evaluation of wells in unconventional reservoirs. The efforts are also useful in evaluating the potential for greenhouse gas (*e.g.* CO_2) injection and storage for mitigating greenhouse gas emissions.

The transport processes in shales that occur from the macro- to molecular-scale was described by Javadpour *et al.* (2007) (Figure 2). Flow of gas at the macroscale, through hydraulic and natural fractures (macro- to micro-scale), is primarily pressure-driven flow (described by Darcy's Law), while flow at finer scales in the shale matrix, through organic and inorganic matter, may occur through a variety of processes including slip-flow and diffusion. While flow at the macro-scale is typically quantified using production (rate-transient) analysis (Clarkson, 2013a, 2013b) and well-test (pressure-transient) analysis (Clarkson *et al.*, 2012a), using transmission of fluids and pressure observations through a wellbore, flow at the micro- and finer scales must be quantified using reservoir samples (core-scale and smaller).

The focus of the current study was on the use of reservoir sample-analysis techniques to characterize pore-structure accessibility and connectivity, which are key controls on fluid flow at the micro- to nano-scale. Imaging techniques may be used to visualize

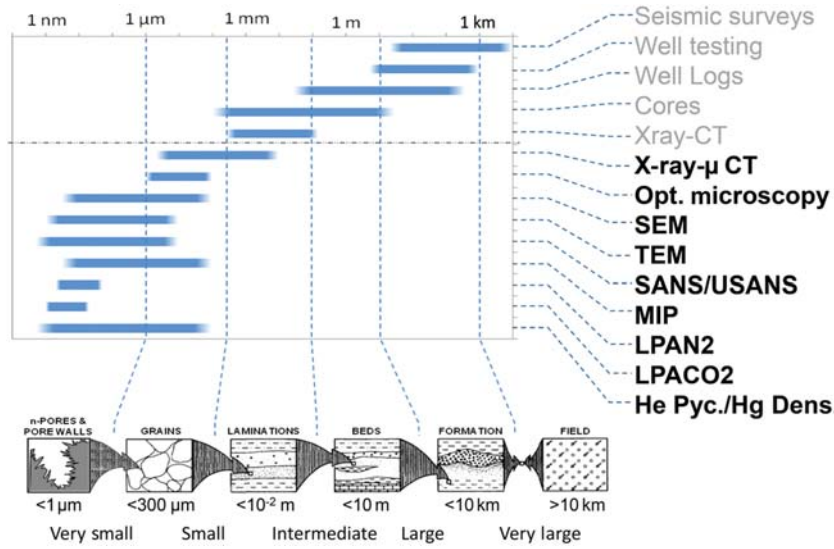

Figure 1. Analytical techniques used to characterize unconventional reservoir properties affecting fluid storage and flow from very large (field) to very small (nano) scale. The methods used by the authors' research group to characterize micro- to nano-scale pore structure and connectivity are highlighted in bold: X-ray-µCT (X-ray micro-computed tomography), optical (petrographic) microscopy, SEM (scanning electron microscopy), TEM (transmission electron microscopy), MIP (mercury intrusion porosimetry), LPAN2 (low-pressure adsorption using nitrogen gas), LPACO2 (low-pressure adsorption using carbon dioxide gas), and He Pyc./Hg Dens. (helium pycnometry to obtain grain density and mercury density – a combination of these densities was used to calculate total porosity) (modified from Krause *et al.,* 1987; Bustin *et al.*, 2008).

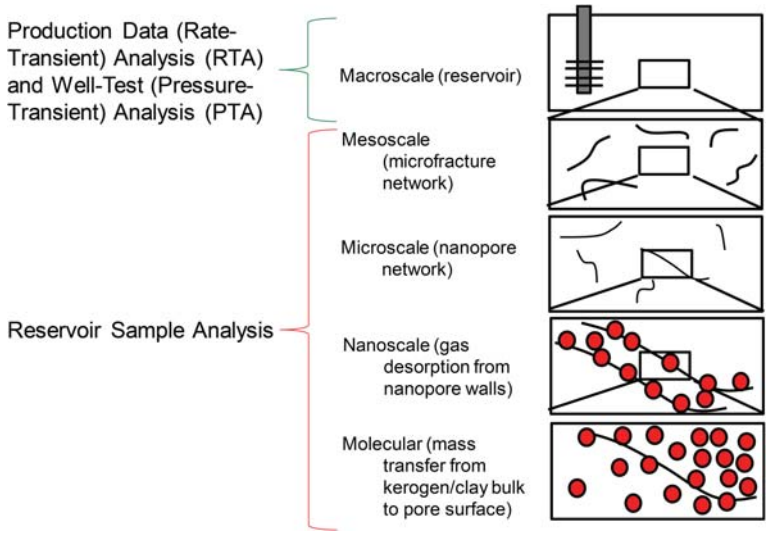

Figure 2. Transport processes occurring from macro- to molecular-scale in shales. Production data (rate-transient) and well-test (pressure transient) analysis are used to characterize flow at the macro-scale, while reservoir samples at core and finer scale are required to characterize flow at the meso- and finer scales (after Clarkson *et al.,* 2012c, modified from Javadpour *et al.*, 2007).

geologic controls at these scales. A mosaic of images gathered using a variety of techniques (Figure 3) was used to illustrate geologic structures and heterogeneities controlling flow. A core-slab photo in the upper left panel (Figure 3) illustrates various elementary lithological components (ELCs) which are lithologies occurring at the cm- to sub-cm scale (bedding, sub-bedding), appearing as patches of different colors [*i.e.* clean litharenites (light brown), argillaceous litharenites (medium brown), and mudstone (dark brown)]. These ELCs have differing levels of porosity and permeability due primarily to variations in grain size and the degree of cementation. X-ray computed tomography (XRCT) imaging performed on core plugs sub-sampled from a larger-diameter core may be used to evaluate bulk-density contrasts occurring at the mm to micron scale, which in turn is useful for assessing porosity distribution (upper right panel). Backscatter electron (BSE) images obtained from SEM can be used for visualization pore structure at the micron- to nano-scale (middle and lower left panels) while transmission electron microscopy (TEM) is useful in imaging nano-scale structures. These latter techniques (SEM and TEM) can also be used for understanding pore association (where the pores reside) and pore morphology; further, SEM images gathered in three dimensions can be useful for understanding pore connectivity at the micron scale. Confirmation and quantification of accessibility and connectivity using fluid invasion (*e.g.* low-pressure adsorption of gases and mercury intrusion) and neutron-scattering methods are desirable.

In previous research (Solano *et al.*, 2014), the volumetric distribution of ELCs (Figure 3, upper left panel) at the core scale (slabbed, full diameter core) was quantified

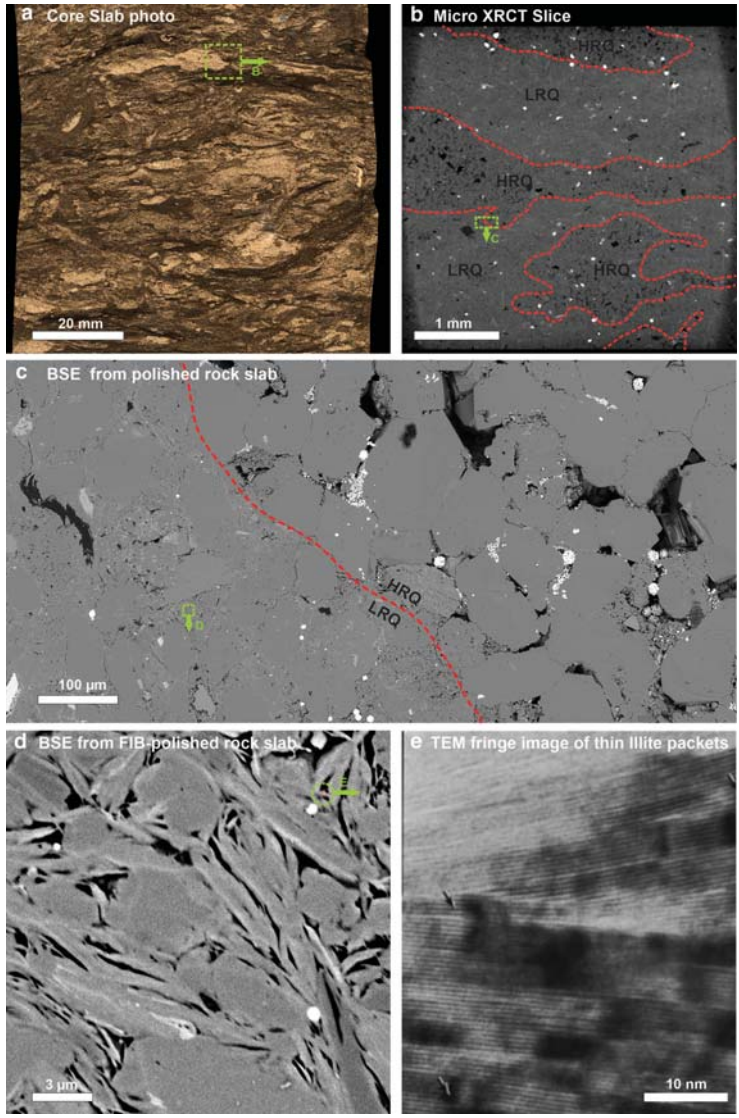

Figure 3. Use of imaging methods to visualize geologic structures controlling flow at core- and finer scale. Core photography (a) is used for imaging the distribution of elementary lithological components, and X-ray micro-computed tomography (b) for imaging bulk-density contrasts and patches of dissimilar reservoir quality in core plugs (sampled from a large whole-core sample). Panels c and d illustrate the use of backscatter imaging from scanning electron microscopy (SEM) for imaging micro- to nano-scale pore structures and their associations. Panel e illustrates the use of transmission electron microscopy (TEM) for imaging nano-scale structures (Jiang *et al.*, 1997). Pores and porous regions in the XRCT and BSE/SEM images are represented by the darker areas. HRQ = high reservoir quality; LRQ = low reservoir quality. All images (except for TEM) were taken for reservoir samples obtained from a tight oil reservoir within the Cardium Formation (Pembina Field) in western Canada.

using a combination of digital photography and XRCT. Reservoir quality indicators, porosity and permeability, obtained through use of XRCT and pressure-decay profile permeability (PDPK) measurements, respectively, were then mapped across the slabbed core face (Figure 4). The XRCT-derived bulk densities were converted to porosity estimates using standards; PDPK measurements were performed on a 5 mm × 5 mm grid to create a 2D permeability map across the slabbed core face (details of this procedure were provided by Solano *et al.* (2014). The resulting 2D map can be used to understand connectivity between ELCs and reservoir-quality differences between them, and their controls on full-diameter core permeability tests. However, in order to gain an understanding of micro-/nano-structural controls on reservoir quality within ELCs, additional analytical measurements are required. For this purpose, a combination of small and ultra-small angle neutron scattering

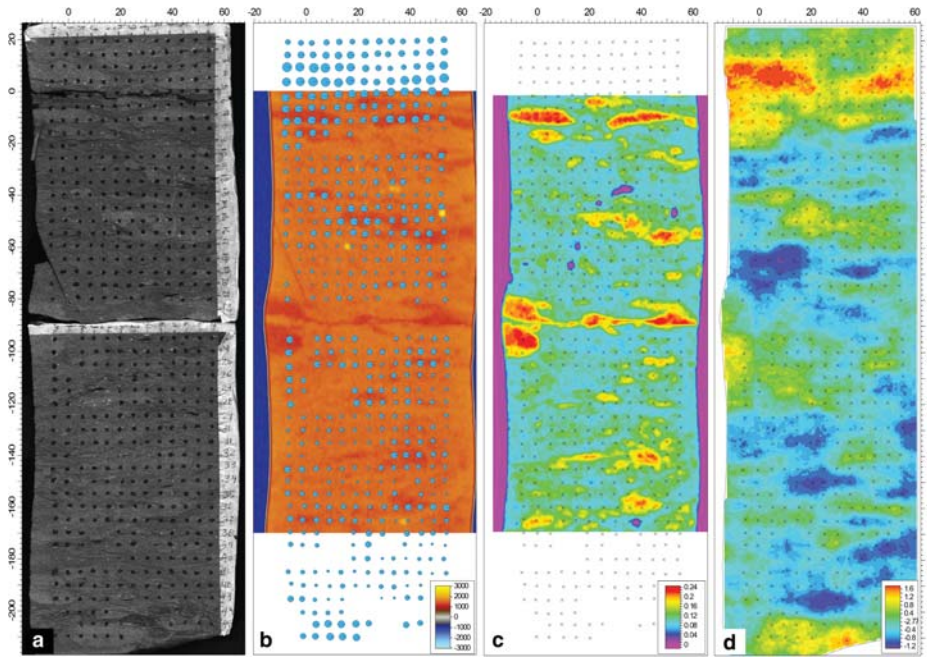

Figure 4. Use of XRCT and PDPK to provide a 2D map of porosity and permeability of a slabbed core obtained from a Pembina Cardium tight oil reservoir. Panel a is a photograph of a core slab surface and shows a two-dimensional grid indicating the location of permeability measurements using a profile permeameter tool (PDPK). Panel b is a virtual representation of panel a on which the color scale represents attenuation of X-ray transmitted intensities (in Hounsfield units) as extracted from an X-ray computed tomography dataset collected from the core to the left (before slabbing it). The size of the blue circles superimposed on this image is proportional to the permeability measured on each spot. Panel c displays a 2D map of porosity values obtained from the X-ray computed tomography. Panel d shows the two-dimensional distribution of permeability across the core slab surface, with the color scale presented as Log (permeability, mD) (modified from Solano *et al.*, 2014).

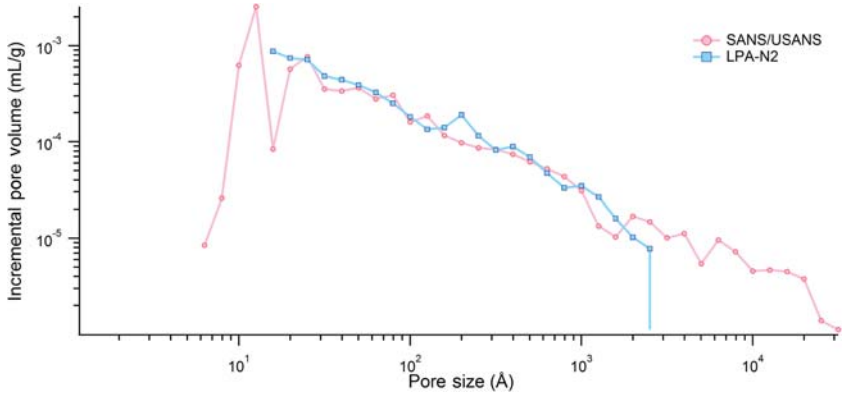

Figure 5. Comparison of pore-size distributions obtained from low-pressure adsorption with N2 (LPA-N2) and small/ultra-small angle neutron scattering (SANS/USANS) (modified from Clarkson *et al.*, 2012b).

(SANS/USANS), mercury intrusion porosimetry (MIP), and low-pressure adsorption (LPA) for 'bulk' property estimation (*i.e.* porosity and pore-size distribution) was used, while imaging techniques (BSE-SEM) were used to understand pore-structure association.

Previous work by the Clarkson research group (Clarkson *et al.*, 2012b; Clarkson *et al.*, 2013) has focused mostly on comparisons of pore-size distributions obtained from LPA and SANS/USANS. These comparisons have been favorable for the most part, as illustrated in Figure 5 and discussed by Clarkson *et al.* (2012b). For conventional and unconventional reservoirs, however, mercury intrusion methods are more commonly used to assess reservoir quality, through attainment of pore-throat distributions (a more direct indicator of permeability) and permeability. Furthermore, the shape of the intrusion profile may be used to evaluate the connectivity of the pores in different pore-size ranges. The focus of the current work was, therefore, on the comparison of SANS/USANS and MIP for evaluation of unconventional reservoir pore structure, accessibility, and connectivity.

2. Samples and methods

The samples probed using SANS/USANS techniques corresponded to the two volumetrically dominant rock types in low-permeability, light-oil bearing areas of the Pembina-Cardium pool in west-central Alberta, Canada. Core-plug samples oriented parallel to the bedding planes were extracted from legacy cores using an air-cooled coring bit system (Figure 6); several axial slices were cut from these plugs and micro-machined down to their final geometry (diameter $\approx$ 11 mm, thickness $\approx$ 1 mm) using a dual rotary axis micro-CNC setup.

The SANS/USANS analysis was focused primarily on samples obtained from two wells in the Pembina-Cardium pool (Table 1).

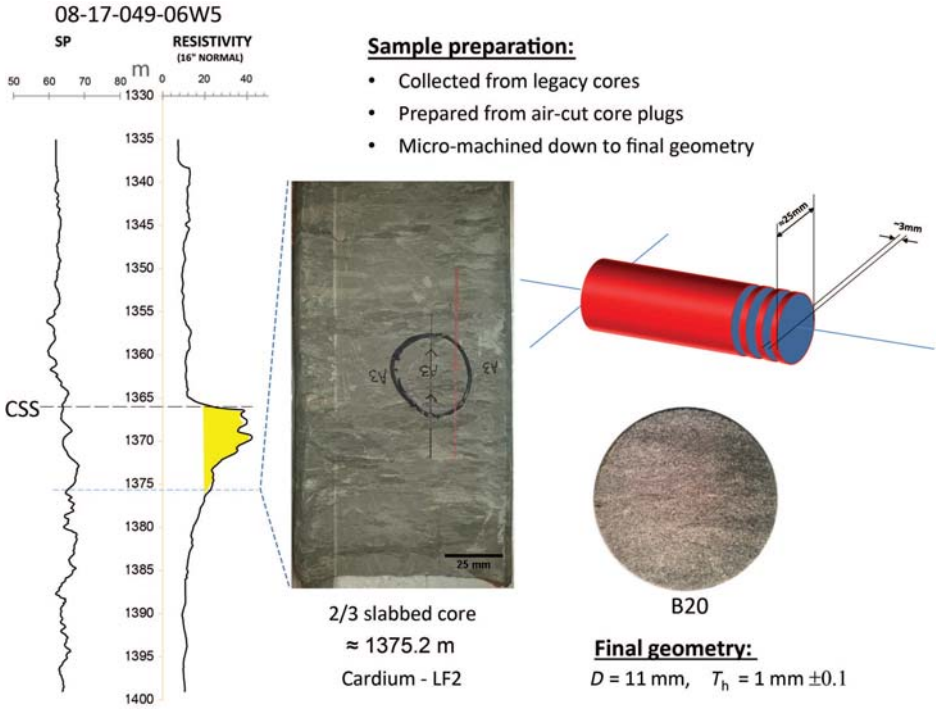

Figure 6. Illustration of selection and preparation of samples for SANS/USANS analysis. Full diameter legacy core samples, located at the base of the Cardium reservoir where lower reservoir quality occurs, were sub-sampled using core plugs.

The SANS experiments were performed on the General Purpose SANS instrument at the Oak Ridge National Laboratory (ORNL, Tennessee, USA), while the USANS experiments were performed at the National Institute for Standards and Technology, using the BT5 perfect crystal SANS instrument. In these experiments, the samples were irradiated with a collimated, monochromatic neutron beam; different detector-source configurations were used to collect small-angle and ultra-small-angle scattering datasets (SANS, USANS, respectively). The aim of these experiments was to gain further understanding of the pore structure and fluid–rock interactions occurring in the nano- to micrometer-sized pores within these rocks. The advantages of using SANS/USANS for pore structure-connectivity studies are: (1) a wide distribution of pore sizes can be

Table 1. Well locations and samples used in the analyses.

Location	Sample	Analysis
08-17-049-06W5	1101A2	SANS/USANS
	1102A1	SANS/USANS
06-05-049-06W5	B20	SANS/USANS
	S01	MIP
	S07	MIP

investigated (~1–10,000 nm); (2) measurements can be performed at elevated temperatures and pressures, simulating reservoir conditions; and (3) connected *vs.* unconnected porosity may be investigated.

Experimental procedures for obtaining porosity/pore-size distributions under ambient conditions followed those described by Clarkson *et al.* (2012b, 2013). Porosity, pore-size distribution (PSDs), and specific surface area (SSA) were calculated using a polydisperse sphere model (PDS) to represent the pore system in the rocks (Radlinski *et al.*, 2004).

Additional experiments were conducted on selected samples using the neutron contrast-matching technique (Melnichenko *et al.*, 2012) in order to investigate the degree of accessibility of the pore network to CO_2 as a function of pore size. CO_2 was used in order to further our understanding of CO_2 storage in tight rocks. For this purpose, multiple scans of each sample were also performed using a high-pressure cell designed at ORNL under varying CO_2 pressures to establish the zero average contrast pressure – the residual scattering at this pressure, combined with the procedures of Melnichenko *et al.* (2012), was used to determine the amount of (unconnected) porosity inaccessible to CO_2.

Mercury intrusion porosimetry data were also collected on equivalent samples to allow comparison with synthetic MIP curves generated from SANS/USANS data. The selected samples were processed in a jaw-crusher and sieved to a uniform size fraction of 2–4 mm before being dried in an oven at 105°C for 24 h to remove any liquids and volatiles. Dried and evacuated samples were loaded into a Micromeritics Autopore IV 9520 porosimeter on which mercury intrusion was measured at constant pressure steps up to 413.7 MPa. The measurements were conducted by Trican Geological Solutions in Calgary, Canada. Pore diameters were determined based on the Washburn equation assuming a mercury surface tension of 485 dynes/cm and a contact angle of 130°.

Additional insights regarding the pore system and mineralogical composition of these rocks were obtained through electron microscopy imaging using an FEI Quanta 250 FEG field emission scanning electron microscope. Different detectors installed on this instrument allowed for the compilation of high-resolution cathodoluminescence (CL), secondary- and backscattered-electron images (SE and BSE, respectively), as well as chemical elemental maps on polished rock surfaces. An additional set of BSE images was collected on two argon ion-milled samples through a commercial laboratory.

3. Results

Combined SANS/USANS datasets were collected from the Cardium samples to analyze the pore structure and connectivity/accessibility of these pores. Combined SANS/USANS scattering profiles, collected at ambient conditions for two samples from different Cardium lithofacies, are shown in Figure 7. The scattering intensity profiles appear to follow a negative slope of 3 on a log–log scale, which indicates a power-law scattering characteristic of a very rough (fractal) pore–matrix interface (Schmidt, 1982; Texeira, 1988; Clarkson *et al.*, 2013). Qualitatively, these scattering profiles appear similar to those observed previously for shales (Clarkson *et al.*, 2013).

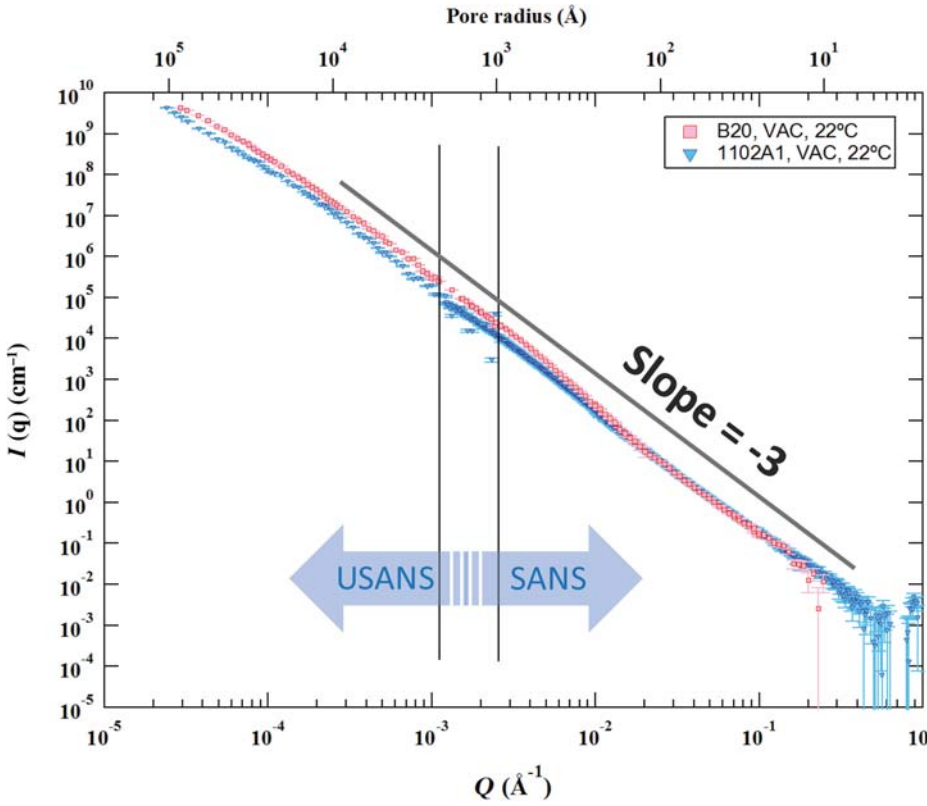

Figure 7. Combined SANS/USANS profiles for two Cardium Fm. samples with contrasting reservoir quality (B20 – high quality, 1102A1 – low quality). A slope of −3 is provided for reference. Pore radius (r) is expressed as a function of the scattering angle (Q) in the upper horizontal axis according to the expression $r = 2.5/Q$.

The processed scattering data for the samples in Table 1 were converted to a PSD (Figure 8a), using the PDS model and the same values of interfacial tension and contact angle used for the actual mercury porosimetry data. The results of the PDS model application are given in Table 2. Equivalent mercury intrusion porosimetry curves are provided in Figure 8b.

SANS/USANS-derived specific surface area ranges between 4 and 27 m^2/g. Three major pore-size regions can be observed from the PSD plots, one in the sub-nanometer region, another in the meso-pore region, and the third encompassing larger pores and centered at ~300 nm. For comparison purposes, MIP-derived PSD and capillary pressure data were also included for two crushed rock samples from adjacent intervals representing ELCs similar to those of samples 1101A2 (sample S07) and B20 (sample S01) (see Table 1 for details). Comparing SANS/USANS- and MIP-derived PSDs (Figure 8a), SANS/USANS is seen to provide more detail in terms of short-range

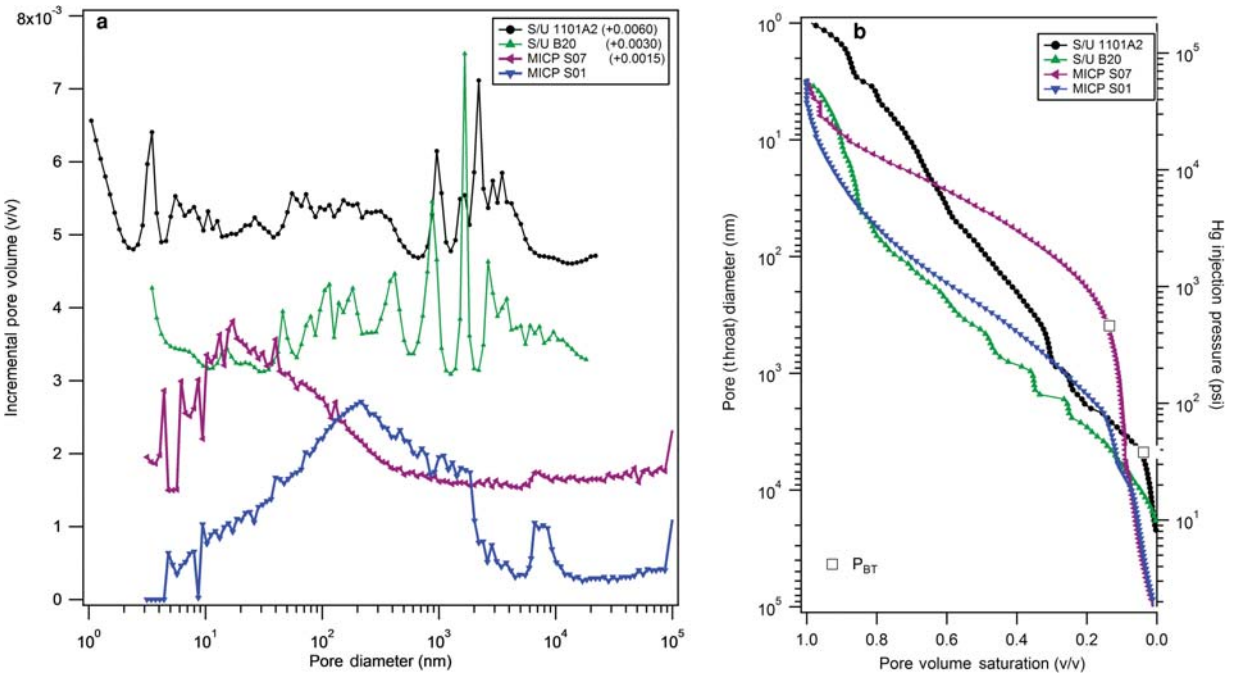

Figure 8. Pore-size distribution (PSD) obtained from small/ultra-small angle neutron scattering (SANS/USANS) and mercury intrusion porosimetry are shown in plot a for several samples from the Cardium Fm.; the curves have been shifted up for clarity as indicated on the legend. Mercury intrusion profiles are shown in plot b for the same samples, S01 and S07, and including equivalent Hg-capillary pressure calculated from processed SANS/USANS data for the other two samples.

Table 2. Results of the analysis of SANS/USANS data for some of the samples using the PDS model (Radlinski *et al.*, 2004).

Location	Sample	PHI (v/v)	SSA (m^2/g)
08-17-049-06W5	1101A2	0.104	37.1
06-05-049-06W5	B20	0.073	4.33

variations in the PSD, and extends further into the small-size side of the spectrum. Comparing synthetic (SANS/USANS) and actual MIP capillary pressure curves (Figure 8b), the actual MIP curves appear to suggest a greater initial entry (breakthrough) pressure (high pressures at low saturated pore volume, labeled as 'P_{BT}') compared to the SANS/USANS-derived curves. High breakthrough pressure on the crushed rock samples might be associated with clusters of discrete pores with relatively large size, which are partly connected (or totally unconnected) to the sample's surface.

In order to gain further understanding of pore connectivity, accessibility of CO_2 to the pore network as a function of pore size was investigated for one of the samples in the USANS region (100 nm to 10 μm). Within this range, the accessible porosity represents $<80\%$ of the total pore volume for a given pore size. Moreover, these preliminary results suggest that relatively larger pores are less accessible to the injected gas (Figure 9). A similar trend was observed previously using the same technique on a moderately mature coal sample (Melnichenko *et al.*, 2012), and on a sample of the Barnett shale (Clarkson *et al.*, 2013). This somewhat puzzling result is explored further in the Discussion section below.

4. Discussion

Traditionally, mercury intrusion data have been used for both conventional and unconventional reservoirs to evaluate reservoir quality at the core scale, providing estimates of pore-throat distributions and permeability. The shape of capillary pressure curves generated from mercury intrusion can also be used qualitatively to assess reservoir quality (Figure 10). From Figure 10, poor-quality (low permeability and porosity) reservoirs are seen to be characterized by high entry pressures and steep capillary pressure curves, while higher-quality reservoirs are characterized by low entry pressure and flatter capillary pressure curves. Referencing the actual MIP curves available for this study (Figure 8), the S01 is expected to have greater reservoir quality than the S07 sample; indeed, the S01 sample has larger pore throats relative to the S07 (see Figure 8).

Comparing MIP and SANS/USANS data for PSD and connectivity/accessibility information, some important inconsistencies are observed. Differences in PSDs are easily explainable: both techniques utilize fundamentally different measurement and physical principles in their interpretation; SANS/USANS have a much wider range of investigation; MIP provides pore-throat distributions *vs.* pore-size distributions for SANS/USANS; some distortion of the pore structure may occur with MIP due to high-pressure intrusion, particularly for small pore sizes; the assumption of a polydisperse sphere pore structure for SANS/USANS *etc*. Differences in interpretation of

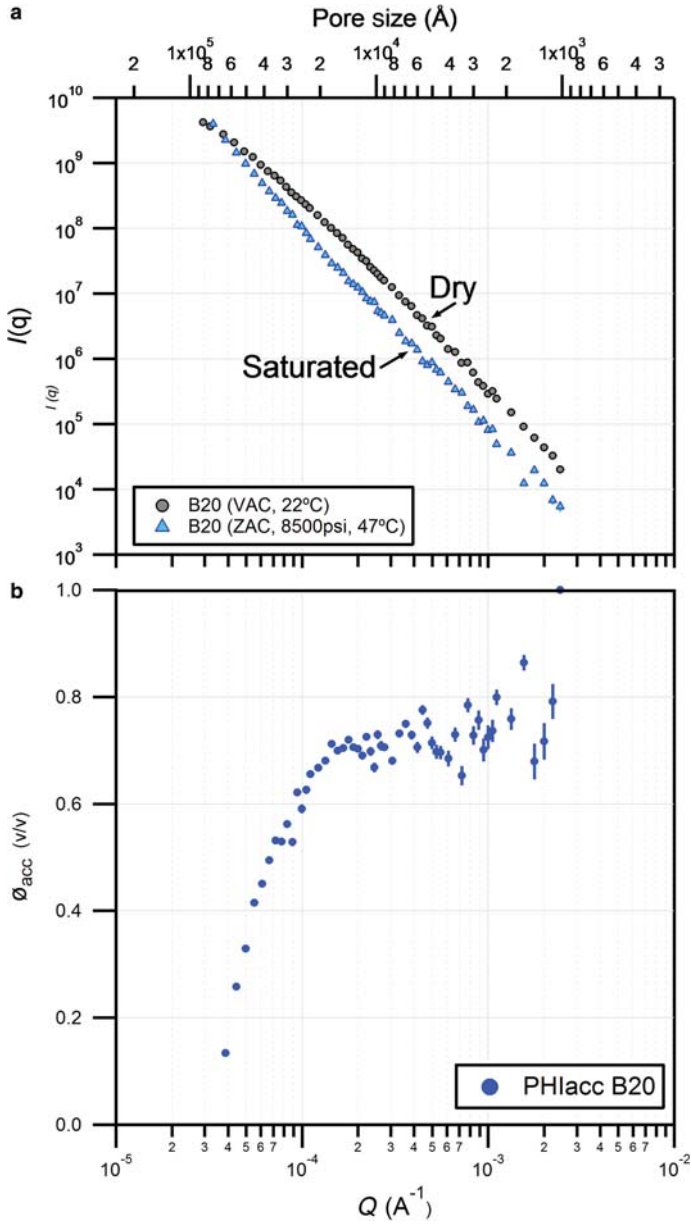

Figure 9. Processed USANS data showing the ratio of accessible to total porosity calculated for two low-permeability samples from the Cardium Fm. Interestingly, this curve suggests that pores >2 μm are less accessible to CO_2 than the smaller pores (<2 μm), where there is more or less a constant ratio of accessible pores from between 55 and 80% of the total porosity.

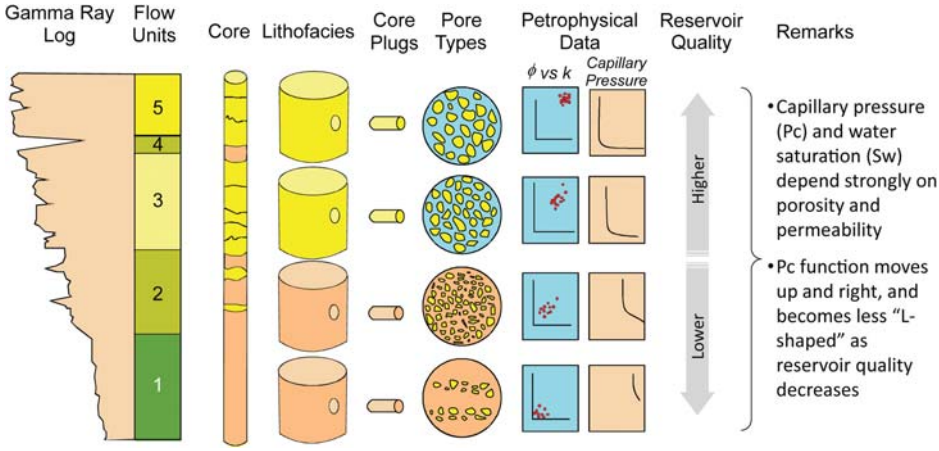

Figure 10. Impact of reservoir quality on petrophysical data. The shape of capillary pressure curves, commonly derived from mercury-intrusion, is significantly affected. Low-quality reservoirs typically have higher entry pressures and steep capillary pressure curves.

pore accessibility/connectivity are more difficult to explain. Comparing the synthetic and actual MIP curves (Figure 8), while the actual MIP curves are seen to have a relatively high entry pressure (pressure at which the internal pore structure of sample is accessed), followed by a slow increase in pressure with saturation, the synthetic curves (derived from SANS/USANS) have a smaller entry pressure and a more rapid increase in pressure with saturation. The difference may be due to the dissimilarity in sample size and preparation; the actual MIP curves were collected on crushed samples (2–4 mm) *vs.* small discs for the synthetic curves. Even though the largest pores in these samples might reach up to 200 μm across, these pores may be isolated or form small clusters; smaller pores are quite likely to have been intruded before these larger pores are accessed, thus creating a shift of the PSD toward smaller pore sizes.

Similarly, several possible explanations exist for the large percentage of inaccessible pores interpreted from the USANS data (Figure 9). So far, three possible explanations have been found for the 'unconnected' porosity interpreted for the larger portion of the pore-size spectrum: (1) actual unconnected pores, probably representing fluid inclusions mainly within mineral grains such as quartz and partly-etched chert; (2) errors in scattering-length density (SLD) calculations, leading to further errors in the SANS/USANS data interpreted. The SLD calculation is a critical component of the porosity/SSA/PSD calculations using SANS/USANS, and is typically based on an 'average' mineral-phase composition. Within the samples, mineral grains/crystals may occur which have a scattering length density (SLD) that is substantially different from the average mineral phase in the sample. These mineral grains/crystals might be embedded inside larger grains representing solid mineral inclusions, although they are more commonly associated with the surrounding matrix as part of a fine-grained detrital component or even as a diagenetic product. (3) A combination of explanations 1 and 2.

The authors are currently investigating these possibilities using a combination of imaging methods (SEM, micro-XRCT), petrographic methods (chemical element mapping using EDX), and SANS/USANS/MIP.

In support of explanation 1, high-resolution SEM images were collected for two Cardium samples the surfaces of which were treated using a Broad Argon Ion Mill system (Figure 11). The images have a resolution of 5 nm per pixel, which allowed for the quantification of structurally intact nm-sized pores even within the clay-rich matrix filling the intergranular pore system. As anticipated from PSDs gathered from SANS/USANS/MIP (Figure 8a), the majority of pores are sub-micrometer scale and located within the clay-rich matrix. These pores exhibit tabular, elongated, and/or triangular cross-sections as a result of the collapse of clay laminae. Although less common, irregularly shaped pores were also observed and were mostly associated with detrital fine- to very fine sand- and silt-sized chert grains and quartz. With the aid of high-resolution SEM imaging, therefore, a possible source of unconnected porosity can be said to exist within quartz and slightly altered chert fragments. Further evidence includes the presence of small cubic crystals deposited adjacent to some of these pores; these are interpreted to be NaCl crystals formed after the pore was opened during the ion-milling process, exposing the encased NaCl-brine to a vacuum atmosphere.

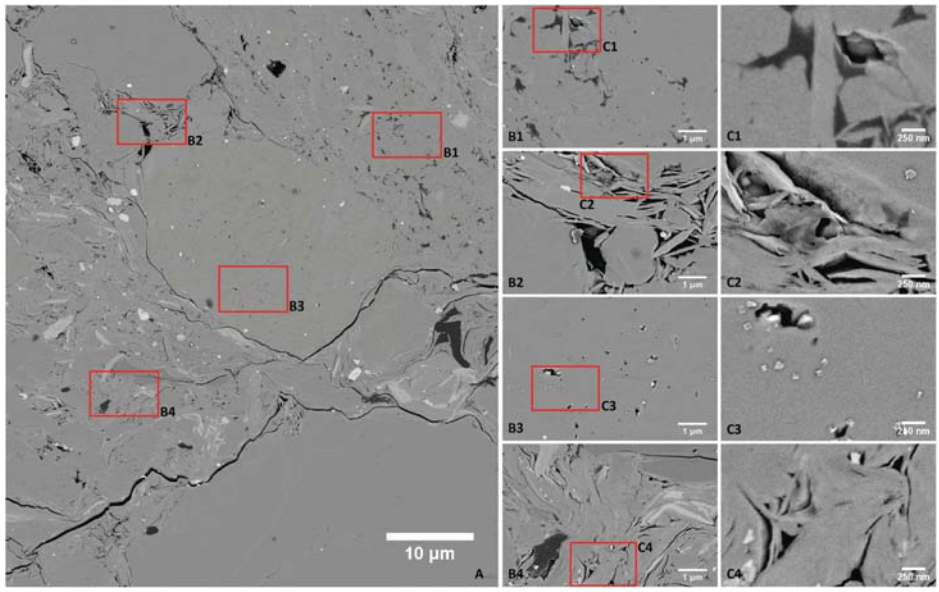

Figure 11. SEM images collected from an ion-milled sample from the Cardium Fm. Locations marked on the index image to the left are enlarged in the central column (B1–B4) with subsequent magnification of selected areas from the latter provided in the right column (C1–C4). This montage highlights the dominant pore geometries observed: (a) irregular pores (B1, C1, B3, and C3); and (b) elongated/tabular and triangular-shaped pores (B2, C2, B4, and C4). Note the presence of small cubic crystals precipitated adjacent to presumably disconnected, brine-filled pores, potentially exposed during the ion-milling process.

In support of explanation 2, chemical element mapping (EDX) was performed of samples analyzed with SANS/USANS to identify rock components possibly affecting SLD calculations. The reason for this investigation is that the SLD is influenced by the spatial distribution and volume fraction of inhomogeneities which give rise to the neutron scattering contrast during a SANS/USANS experiment. The SLD values for rock samples are usually calculated for the solid fraction *via* XRD-extracted mineralogical compositions, which are then combined with published values of bound coherent neutron scattering lengths for the corresponding atoms within the quantified minerals. A direct consequence of this procedure is that only an average SLD value can be obtained for a given sample; moreover, quantification limits from XRD analysis are usually $>3\%$ (w/w), so mineral phases present in smaller quantities cannot be included accurately (if at all) in the analysis. The SLD calculation using this conventional procedure can, therefore, be in significant error for highly heterogeneous rocks. Chemical-element mapping may provide an important source of information to complement the petrographic and mineralogical characterization of these samples.

From EDX mapping of the SANS/USANS samples, four primary components contributing to the neutron scattering contrast were identified: (1) pores (either connected or unconnected); (2) Ti oxide (probably anatase); (3) an ensemble of silicates (quartz, feldspars, clays, *etc*.); and (4) Fe carbonate (probably siderite). The presence of these four phases partially impairs the usefulness of standard two-phase (pore + average mineral phase) system models, with direct impact on the quantification of total porosity, PSD, and connected *vs.* unconnected porosity from the associated datasets. A possible method to address this limitation consists of the characterization of geometry and spatial distribution of these components in the system, which in turn requires greater resolution/quality SEM/EDX datasets. In addition, it would be useful to collect additional datasets using neutron contrast-matching techniques to 'turn off' the scattering signal for each of the individual components, so the problem can be analyzed in terms of a three-phase system (Wu, 1982).

5. Conclusions

Using a combination of SANS/USANS, fluid invasion, and imaging methods, pore structure, accessibility, and connectivity for multiple Cardium Fm. tight oil samples have been investigated. Analysis by SANS/USANS revealed a broad pore-size distribution with pore accessibility varying strongly with pore size. One surprising result was that the accessibility was less for larger pore sizes, although this finding was not inconsistent with the results from mercury intrusion. High-resolution SEM imaging has, in fact, revealed that unconnected pores appear within mineral grains, possibly explaining the SANS/USANS results. The SANS/USANS interpretations may, however, be affected by the assumption of a two-component system (pores + average mineral phase). Mineral mapping using EDX suggests possible additional components which could affect significantly the SANS/USANS-derived porosity, PSD, and pore-accessibility calculations – a multi-component system will be tested

in future studies and differences quantified using the more conventional two-component model.

Acknowledgments

The present research was funded in part by the 'Tight Oil Consortium' (http://tightoil-consortium.com/) at the University of Calgary, and also by the ORNL Postdoctoral Research Associates Program, administered jointly by the ORNL and the Oak Ridge Institute for Science and Education. The elements of this work utilizing the BT-5 instrument at the NCNR were supported in part by the National Science Foundation under agreement No. DMR-0454672. Clarkson thanks Alberta Innovates – Technology Futures, Shell, and Encana for supporting his Chair in Unconventional Gas and Light Oil Research in the Department of Geoscience, University of Calgary, Canada.

Guest editor: Thorsten Schäfer

The authors and editors are grateful to anonymous reviewers who offered very helpful input and suggestions. A list of all reviewers is given at the end of the Preface for this volume.

References

Bustin, R.M., Bustin, A.M.M., Cui, X., Ross, D.J.K., and Murthy Pathi, V.S. (2008) Impact of shale properties on pore structure and storage characteristics. SPE paper 119892, presented at the Society of Petroleum Engineers Shale Gas Production Conference in Fort Worth, Texas, USA, November 16–18, 2008.

Clarkson, C.R. (2013a) Production data analysis of unconventional gas wells: Review of theory and best practices. *International Journal of Coal Geology*, **109–110**, 101–146.

Clarkson, C.R. (2013b) Production data analysis of unconventional gas wells: Workflow. *International Journal of Coal Geology*, **109–110**, 147–157.

Clarkson, C.R., Jensen, J.L., and Chipperfield, S. (2012a) Unconventional gas reservoir evaluation: What do we have to consider? *Journal of Natural Gas Science and Engineering*, **8**, 9–33.

Clarkson, C.R., Freeman, M., He, L., Agamalian, M., Melnichenko, Y.B., Mastalerz, M., Bustin, R.M., Radliński, A.P., and Blach, T.P. (2012b) Characterization of tight gas reservoir pore structure using USANS/SANS and gas adsorption analysis. *Fuel*, **95**, 371–385.

Clarkson, C.R., Nobakht, M., Kaviani, D., and Ertekin, T. (2012c) Production analysis of tight-gas and shale-gas reservoirs using the dynamic-slippage concept. *SPE Journal*, **17**, 230–242.

Clarkson, C.R., Solano, N., Bustin, R.M., Bustin, A.M.M., Chalmers, G.R.L., He, L., Melnichenko, Y.B., Radliński, A.P., and Blach, T.P. (2013) Pore structure characterizaton of North American shale gas reservoirs using USANS/SANS, gas adsorption, and mercury intrusion. *Fuel*, **103**, 606–616.

Javadpour, F., Fisher, D., and Unsworth, M. (2007) Nanoscale flow in shale gas sediments. *Journal of Canadian Petroleum Technology*, **46**, 55–61.

Jiang, W.T., Peacor, D., Árkai, P., Tóth, M., and Kim, J. (1997) TEM and XRD determination of crystallite size and lattice strain as a function of illite crystallinity in pelitic rocks. *Journal of Metamorphic Geology*, **15**, 267–281.

Krause, F.F., Collins, H.N., Nelson, D.A., Machemer, S.D., and French, P.R. (1987) Multiscale anatomy of a reservoir: geological characterization of Pembina-Cardium Pool, west-central Alberta, Canada. *AAPG Bulletin*, **71**, 1233–1260.

Melnichenko, Y.B., He, L., Sakurovs, R., Kholodenko, A.L., Blach, T., Mastalerz, M., Radliński, A.P., Cheng, G., and Mildner, D.F.R. (2012) Accessibility of pores in coal to methane and carbon dioxide. *Fuel*, **91**, 200–208.

Radlinski, A.P., Ioannidis, M.A., Hinde, A.L., Hainbuchner, M., Baron, M., Rauch, H., and Kline, S.R. (2004) Angstrom-to-millimeter characterization of sedimentary rock microstructure. *Journal of Colloid and Interface Science*, **274**, 607–612.

Schmidt, P.W. (1982) Interpretation of small-angle scattering curves proportional to a negative power of the scattering vector. *Journal of Applied Crystallography,* **15**, 567–569.

Solano, N.A., Krause, F.F., and Clarkson, C.R. (2014) Characterization of cm-scale heterogeneities in a tight oil reservoir using X-ray computed tomography, profile permeability measurements and 3-D image analysis. Paper URTeC 1922810 presented at the Unconventional Resources Technology Conference held in Denver, Colorado, 25–27 August 2014.

Teixeira, J. (1988) Small-angle scattering by fractal systems. *Journal of Applied Crystallography,* **21**, 781–785.

Wu, W.-I. (1982) Small-angle X-ray study of particulate reinforced composites. *Polymer,* **23**, 1907–1912.